

**Characterizing Collisions Between Ultracold Rb and Cold
OH in Dual Electromagnetic Trap**

by

W. J. Solorio Hernandez

A thesis submitted to the
Faculty of the Honors Committee of the
University of Colorado at Boulder
Bachelor of Arts
Department of Physics, Defended March 11 2024
2024

Committee Members:

Thesis advisor: Heather Lewandowski, Physics Department

Outside Reader: David Brain, APS Department

Honors Council Representative: John Cumalat, Physics Department

Solorio Hernandez, W. J. (B.A., Physics)

Characterizing Collisions Between Ultracold Rb and Cold OH in Dual Electromagnetic Trap

Thesis directed by Prof. Thesis advisor: Heather Lewandowski, Physics Department

The interactions between cold and ultracold molecules can provide crucial insights into the chemistry of extreme environments, the transition from classical to quantum reaction dynamics, and precision measurements of reactions or fundamental constants. The OH Rb Interactions in Trap (OHRbIT) experiment characterizes elastic and inelastic collisions between magnetically trapped Rb atoms and electrically trapped OH molecules by transporting magneto-optical trapped Rb atoms to the slowed OH molecules. Inelastic collisions cause trap loss while elastic collisions promote sympathetic cooling through thermal equilibrium. In this thesis, I describe the required alignment preparation of the traps and clouds, as well as preliminary results of the inelastic cross section of OH-Rb collisions and the Rb distribution in the dual trap over time.

Dedication

To my family.

Acknowledgements

I would like to thank my advisor Heather Lewandowski for all of the support she has provided me this last year. She has provided me with great guidance into the world of cold and ultracold physics, and I am inspired to continue learning more about the field in graduate school. I would also like to thank Tommy Garcia and Stephen Kocheril, who worked with me on the experiment. Tommy was a fantastic mentor who taught me how to operate the experiment and the physics behind it all. Stephen would always be there to help Tommy and me with any issue that crossed our path. Finally, I would like to thank the rest of the Lewandowski group, Olivia, Chase, Trevor, Malayne, and Alicja.

Contents

Chapter	
1	Introduction 1
1.1	Cold Molecules 1
1.2	Sympathetic Cooling of the OH Radical 2
1.3	The Experiment 3
2	Cooling Methods 4
2.1	Ultracold Atoms 4
2.1.1	The Zeeman Effect 6
2.1.2	Magneto-Optical Trap 8
2.1.3	Magnetic Trap of Rb and Transportation 12
2.2	Cold OH Generation 12
2.2.1	Stark Decelerator and Quadrupole Electrostatic OH Trap 14
3	Characterization Methods 18
3.1	Absorption Imaging 18
3.2	Ionization Technique 19
4	Preparation and Measurement of Collisions 21
4.1	Theory and Experiment Expectations 21
4.1.1	Theoretical Models for Sympathetic Cooling 22

4.1.2	Cross Section Expectations	25
4.2	Optimizing Alignment	27
4.2.1	Ionizing Laser Alignment	28
4.2.2	Dual Trap Alignment	29
4.3	Collisions	31
5	Results and Analysis	33
5.1	Characterization of Rb and OH	33
5.2	Inelastic Cross Section	39
6	Conclusion	42
6.1	Summary	42
6.2	Future Work	43

Figures

Figure

- 2.1 Scattering rate plot of photons by an atom. Atoms that are blue-shifted (traveling towards the laser beam) will see the laser frequency closer to resonance, therefore having a higher scattering rate. 5
- 2.2 The beam path of the trapping and repump beams in the experimental setup of the MOT. Both beams are split into six separate beams through the polarizing beam-splitting cube to hit the glass cell with the Rb atoms in orthogonal and counter-propagating directions. Image taken from [6]. 7
- 2.3 (a) The MOT setup. The large arrows represent the trapping laser beams traveling in six directions. The beams are circularly polarized to drive either the σ^+ or σ^- transitions. The quadrupole magnetic field is shown at the center of the trap. (b) This MOT works by inducing the Zeeman effect linearly with position from the center of the trap. As z increases, the energy sublevels increase or decrease in energy. The energy of the trapping light and the direction of their circular polarization are shown at the bottom of the graph. Images taken from [7]. 10
- 2.4 Energy level schematic of Rb-87 showing the wavelength of light between transitions. Figure taken from [6] 11

2.5	(a) Illustration of the moving magnetic trap. The MOT cell is the glass cell in which the Rb atoms are cooled and collected. The dark disks represent the magnetic coils, one on top of the cells and one on the bottom (not pictured). The track moves along the long y dimension and molecular beam direction z. Images taken from [6]. (b) Illustration of the electrostatic trap (the four electrodes on the left), magnetic trap and track (on the top right), and Stark Decelerator (series of black and white electrodes on the far left). Image taken from [3].	13
2.6	Illustration of the generation of cooled OH through supersonic expansion. Figure taken from [3].	15
2.7	Plot of the potential generated from the Stark Decelerator electrode pins. The blue curve is the potential at the configuration where in the series of pins, the first one is set to +12V, the third one is set to -12V, and the second and fourth ones are grounded. The red curve shows the potential when the electrodes are set to an opposite configuration. The dark curve shows the molecules climbing the potentials until the electrode configuration is switched, stealing stark potential (and kinetic energy) as the molecules move through the decelerator. Image taken from [3].	17
4.1	Theoretically calculated inelastic and elastic cross sections in the incident Channel 1 case. Plot also includes the Langevin inelastic cross section for the higher temperature range. Figure taken from [5].	24
5.1	Plot of the number of atoms and peak OD at varying small track positions. The small track position is in micrometers away from the center of the electrostatic trap. Atom number and peak OD are given as a ratio of the number with the electric fields on over the number with the electric fields off at the same track position. Gaussian fits are also shown next to the data points.	34

5.2	Plot of the Rb ion signal from the MCP at varying micromotor positions. The distribution of ions hitting the MCP over a short time was obtained from an oscilloscope. The area under the curve was determined to be the average ion signal (nanovolt seconds). The ion signal is fitted to a double Gaussian curve.	35
5.3	Plot of the number of atoms and peak OD at varying large track positions. The large track position is in micrometers away from the center of the electrostatic track along the y dimension.	37
5.4	(a) Plot of the Rb ion signal (black) and OH ion signal (blue) at the atom x position that gave the best overlap of cloud centers. The atom x position was set to a coil difference of 34 A. (b) Plot of the difference of picomotor scan centers between the Rb and OH over varying x positions of the Rb cloud (controlled by the magnetic trap coil current offset). A linear fit was applied to the data to find the current offset (atom x position) that would yield a picomotor scan center difference of zero.	38
5.5	Plot of the number of atoms over varying time spent in the dual trap with both traps on. The distribution of the number of atoms is fitted to a double exponential decay curve, where the decay time of the slower decay of one curve is used as the lifetime of Rb in the trap.	40
5.6	Plot of the OH signal over two interaction times with and without atoms present. Detect time is the time between the beginning of the OH creation/cooling process and the end of the experiment when the electrostatic trapping fields are turned off.	40

Chapter 1

Introduction

1.1 Cold Molecules

An excellent way to study the physics of matter in extreme conditions is through the study of cold atoms and molecules. Cold molecules can be used for precision measurements, to study elastic and inelastic scattering, to test new phases of matter, and much more [1]. For example, Hudson *et al.* combined measurements of OH megamasers with spectroscopic measurements of OH to constrain the fine structure constant [2]. Another motivation for studying cold molecules has been an interest in learning more about the chemistry and physics of molecules in environments like planetary atmospheres or the interstellar medium. By cooling the molecules, we can prepare them in specific internal states and then study how they interact or react with other molecules or atoms. The OH radical is a molecule of interest in cold molecule research as it is a key ingredient in oxidation reactions, is abundant in Earth's atmosphere, and is extremely reactive [3].

Unlike atoms, molecules have additional rotational and vibrational internal states that complicate the cooling processes. Consequently, an interesting problem in the field of molecular physics is how to deal with the added complexity and bring the molecules to the ultracold temperature regime. One promising solution to create ultracold molecules is to cool the molecules through interactions with ultracold atoms. This process is known as sympathetic cooling, and by studying if it is possible between two species, we can also learn more about the interactions (collisions) between both species of atoms and molecules. There exist several experimental techniques to study cold collisions; experiments either direct a molecular beam onto a trapped species, use crossed or

merged molecular beams, or trap both species in the same location [4]. Each system has its limitations, but experiments that rely on molecular beams suffer from limited interaction times that then limit the collisions that can be measured [4]. On the other hand, the third method of trapping both species, which is known as a dual trap, optimizes the interaction time and density of trapped atoms/molecules. The collisions between the species directly impact how they interact with the trap. Elastic collisions allow for the exchange of kinetic energy which sympathetically cools the hotter species, while inelastic collisions cause changes in the quantum states of the species [4]. The former has the effect of increasing the lifetime of the species in the dual trap while the latter causes the atoms/molecules to fall in anti-trapped states that result in trap loss and a reduction of lifetime. Sympathetic cooling can be an alternative to laser cooling to create ultracold molecules, but for sympathetic cooling to be effective, elastic collisions must be significantly more likely than inelastic collisions. By measuring the collision cross sections for inelastic and elastic collisions between cold molecules and ultracold atoms, we can therefore determine the viability of sympathetic cooling.

1.2 Sympathetic Cooling of the OH Radical

The feasibility of sympathetic cooling for OH molecules with ultracold Rb has been a point of interest in ultracold molecule research [5]. Large amounts of Rb atoms can be readily cooled and trapped in the hundreds of microkelvin temperature regime. On top of that, OH has a hyperfine structure and both species are open-shell doublet species, which makes OH-Rb interactions one of the most notable complex systems to study at low temperatures [5]. Current theoretical calculations use the potential energy surfaces between the OH and Rb to make estimates of the elastic and inelastic cross sections [5]. While theoretical methods can estimate the interaction potentials between colliding species, experimental methods that measure the cross sections can provide corrections to the models in the lower temperature regime [3]. This has been demonstrated before with ND₃ and ⁸⁷Rb, where ultracold rubidium atoms and cold ND₃ molecules were trapped in a dual trap and allowed to interact [4]. Measurements of the OH-Rb interactions have been made before by Gray, however, the results lack robust measurements of the Rb distribution over inter-

action times [3]. As such, to confirm the predicted cross sections calculated by Lara *et al.*, OH-Rb collisions can be once more studied in a dual trap system. To this end, the OH and Rb Interacting in Trap experiment uses a dual electromagnetic trap to confine both species in the same location and allow for the characterization of the elastic and inelastic collision cross sections.

1.3 The Experiment

In this thesis, I discuss the experimental apparatus and preparation procedure for the OH and Rb Interacting in Traps (OHRbIT) experiment to study the collisional cross sections of ^{87}Rb and OH in a dual trap. This thesis is organized in the following way. Chapter 2 discusses The experimental setup used to capture, cool, and transport the atoms and molecules. Then, the common detection methods for atoms and molecules in the vacuum system are discussed in Chapter 3. In Chapter 4, I discuss the theoretical predictions of the cross sections, the expected results from previous work with OHRbIT by Gray, and the procedures used to align the traps and collect collision data. Finally, I discuss the results of the alignment process, preliminary Rb distribution in dual trap measurements, and inelastic cross section calculations in Chapter 5, followed by a summary and discussion of future work in Chapter 6.

Chapter 2

Cooling Methods

The OHRbIT experiment combines two separate systems to cool and transport the atoms and molecules after which they are overlapped for collisions. The Rb atoms are laser cooled through a magneto-optical trap and then moved using a purely magnetic trap that is generated by a pair of electromagnetic coils. When it comes to the molecules, supersonic expansion is used to cool the OH and a Stark Decelerator is used to control the molecular cloud's final position and velocity.

2.1 Ultracold Atoms

The process of creating cooled and trapped atoms through lasers relies on the principle of the scattering force. When an atom absorbs light from a laser, it also absorbs its momentum and, since momentum is conserved, the atom's momentum changes as a result. Atoms, therefore, experience a force in the direction that the laser is propagating in, which is equal to the product of the photon's momentum and the scattering rate. To ensure that the atoms are slowed and not heated by the laser beam, the light is red-detuned. Atoms that are moving towards the laser beam will experience a blue shift, which counteracts the red-detuning and results in a higher scattering rate. As a result, atoms that are moving toward the laser beam and will be therefore cooled have a higher scattering rate than atoms moving away from the beam (see 2.1).

Scattering of photons by an atom:

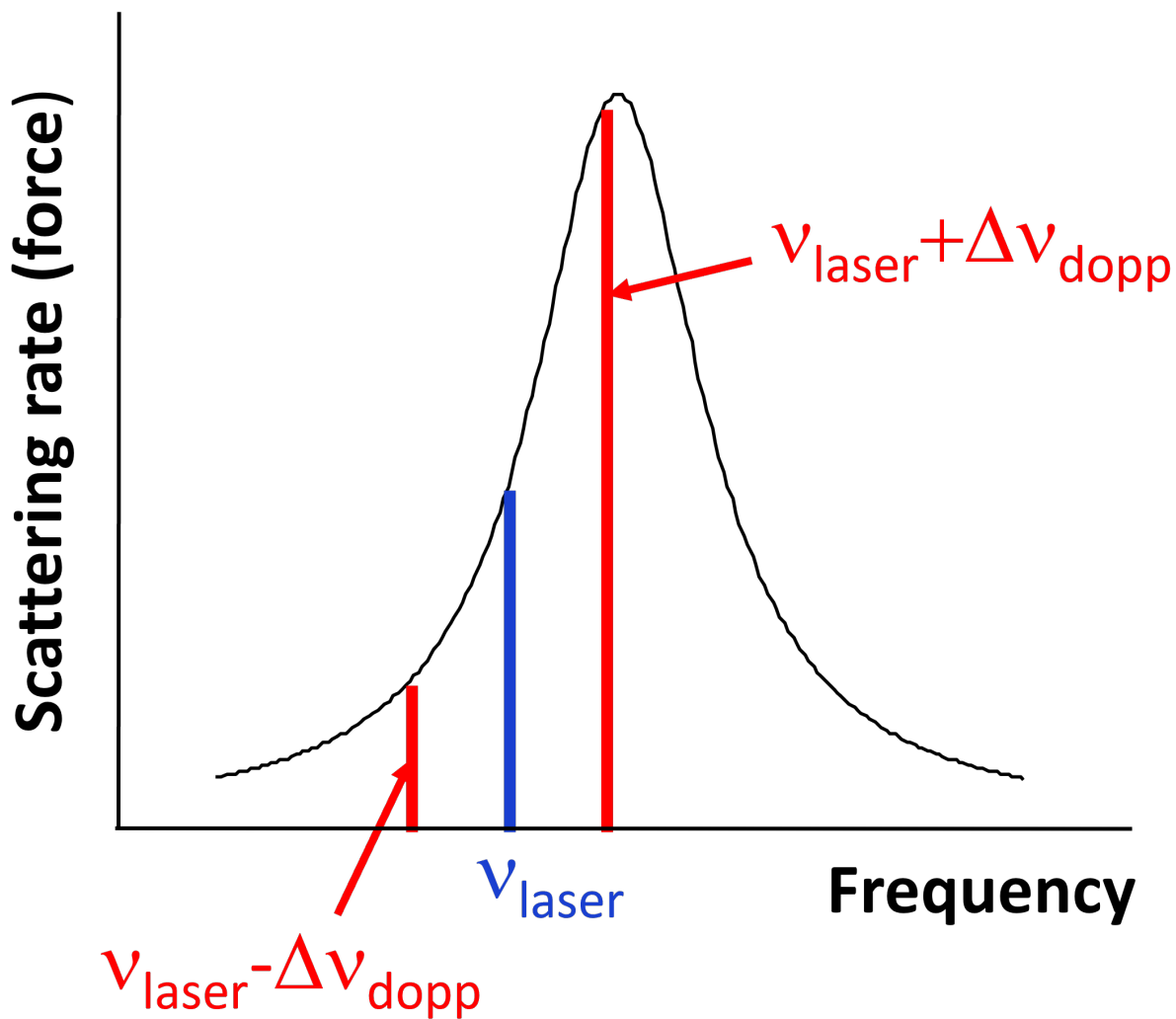


Figure 2.1: Scattering rate plot of photons by an atom. Atoms that are blue-shifted (traveling towards the laser beam) will see the laser frequency closer to resonance, therefore having a higher scattering rate.

2.1.1 The Zeeman Effect

To cool a cloud of atoms, the cloud must be hit in all directions by cooling laser beams (Figure 2.2). As the atoms reach lower velocities, the relativistic effect of Doppler shifting brings the atoms out of resonance with the laser, so atoms eventually stop absorbing light [7]. This method of slowing the atoms is called an optical molasses, and atoms typically diffuse out on the order of a few seconds. We can convert the optical molasses into a trap by taking advantage of the Zeeman effect of a weak magnetic field. The Zeeman effect refers to the splitting of the energy levels of an atom in the presence of an external magnetic field. For rubidium, we consider the hyperfine structure, where the interaction between the atom's nuclear magnetic moment $\boldsymbol{\mu}_I$ and the magnetic flux density generated by the atom's electrons results in the following Hamiltonian:

$$H_{\text{hyperfine}} = -\boldsymbol{\mu}_I \cdot \mathbf{B}_e = g_I \mu_N \mathbf{I} \cdot \mathbf{B}_e, \quad (2.1)$$

where g_I is the g factor, μ_N is the nuclear magneton, and \mathbf{I} is the nuclear spin. By introducing an external magnetic field, the Hamiltonian of the atom changes to reflect the interaction between the atom's total magnetic moment $\boldsymbol{\mu}_{\text{atom}}$ and the external magnetic field \mathbf{B} . The atom's total magnetic moment can be written as the sum of its nuclear and electronic magnetic moments, which are related to nuclear spin \mathbf{I} and electron total angular momentum \mathbf{J} as

$$\boldsymbol{\mu}_{\text{atom}} = -g_J \mu_B \mathbf{J} + g_I \mu_N \mathbf{I}. \quad (2.2)$$

Here, μ_B is the Bohr magneton and is much greater than μ_N , so we neglect the nuclear contribution. The Hamiltonian is therefore given by

$$H = g_J \mu_B \mathbf{J} \cdot \mathbf{B}, \quad (2.3)$$

where g_J is the g-factor [7].

To use the Zeeman effect to trap the atoms, we use a weak external magnetic field. This means that the interaction with the external magnetic field is weaker than the hyperfine interaction of 2.1. As a result, the \mathbf{J} and \mathbf{I} vectors move around their sum vector \mathbf{F} , meaning that M_I and M_J

are no longer good quantum numbers. Instead, we use F and M_F . The Hamiltonian then becomes the following after taking the projection of \mathbf{J} along \mathbf{F} :

$$H = g_J \mu_B \frac{\langle \mathbf{J} \cdot \mathbf{F} \rangle}{F(F+1)} \mathbf{F} \cdot \mathbf{B} = g_F \mu_B B F_z, \quad (2.4)$$

where g_F accounts for the projection of \mathbf{J} onto \mathbf{F} . Similarly, the Zeeman energy is given by

$$E = g_F \mu_B B M_F. \quad (2.5)$$

This energy is proportional to magnetic field strength B , so near the center of a quadrupolar magnetic field where the magnetic field can be approximated as linear, the energy shift due to the Zeeman effect is linear with position.

2.1.2 Magneto-Optical Trap

In this experiment, we use a quadrupolar magnetic field generated by Anti-Helmholtz coils to induce the weak field Zeeman effect (Figure 2.3a). This type of trap is known as a magneto-optical trap (MOT). Despite the magnetic fields, the laser beams provide the trapping force in MOTs. The point of the magnetic fields is to induce the Zeeman effect on the atoms such that the scattering forces become imbalanced. To see this, consider the quantum number J , which is the total angular momentum of the atom in the fine structure case, so J is the sum of electron spin and orbital angular momentum. Similar to Equation 2.5, the Zeeman effect changes the M_J sublevels to be linear with position. For the $J = 0$ to $J = 1$ transition, atoms that move in the positive z direction will be in the $M_J = -1$ sublevel as a result of selection rules. This sublevel is resonant with the trapping beam at some distance away from the center of the trap, so when the atom reaches this point the trapping laser beam photons will be absorbed. The scattering photon force then pushes the atom back to the center of the trap. The trapping laser beams must be circularly polarized so that when the photons hit the atoms, the photons impart the correct positive or negative angular momentum to excite the atoms. For example, atoms in the $M_J = -1$ state can only be excited to the $M_J = 0$ state, so the trapping laser beam must impart positive angular momentum along the

quantization axis. Consequently, only photons of σ^- polarization will be absorbed by atoms that are some distance z to the right of the trap center (Figure 2.3b).

The same MOT principles apply in the hyperfine structure, where the linear perturbation of the M_F sublevels by the Zeeman effect is seen in Equation 2.5. We use a MOT to cool and trap the Rb atoms to the ultracold temperature regime. For ^{87}Rb , the fully stretched low magnetic field seeking state is the $F = 2$, $M_F = 2$ state. Low field-seeking states refer to states in which the energy of the atom/molecule increases with the magnitude of the field. We want as many of the atoms to be in this state since this state is magnetically trappable, which is ideal since we can then use a magnetic trap to move the atom cloud around the vacuum system. To create the MOT, the atoms are excited to the $F' = 3$ state from the $F = 2$ state using a 780 nm external cavity diode laser. For Rb, F refers to the total angular momentum quantum number of the Rb in the $5S_{1/2}$ energy level while F' refers to the total angular momentum quantum number of Rb in the $5P_{3/2}$ energy level (Figure 2.4). Two laser beams are used to create the trapping forces on the atoms, which are the trapping beam and the repump beam. A repump beam excites atoms from the $F = 1$ into the $F' = 2$ state. This is done to account for atoms that happen to start in or de-excite into the $F = 1$ state, meaning that the repump beam repopulates the number of Rb atoms in the $F = 2$, $M_F = 2$ state. The beams are generated by two separate 780 nm external cavity diode lasers. The trapping beam goes through a series of beam-splitting cubes, half-wave plates, and quarter-wave plates as depicted in Figure 2.2. The trapping beam is circularly polarized by the quarter-wave plates to direct the excitations of the atoms towards the $F = 2$, $M_F = 2$ state. The beams intersect a cylindrical glass cell in the laboratory vertical axis (x), large track axis (y), and molecular beam axis (z), for a total of two trapping beams per direction. The glass cell is connected to the rest of the experiment and is under low pressure, and is also where Rb vapor is generated from Rb filament dispensers called Rb getters. The quadrupole magnetic field is generated by a pair of electromagnetic coils that are mounted onto two tracks which can move along the molecular beam axis and the large track axis (Figure 2.5a). The tracks and coils are outside the vacuum chamber. The same coils that generate the magnetic field for the MOT are also used for the pure

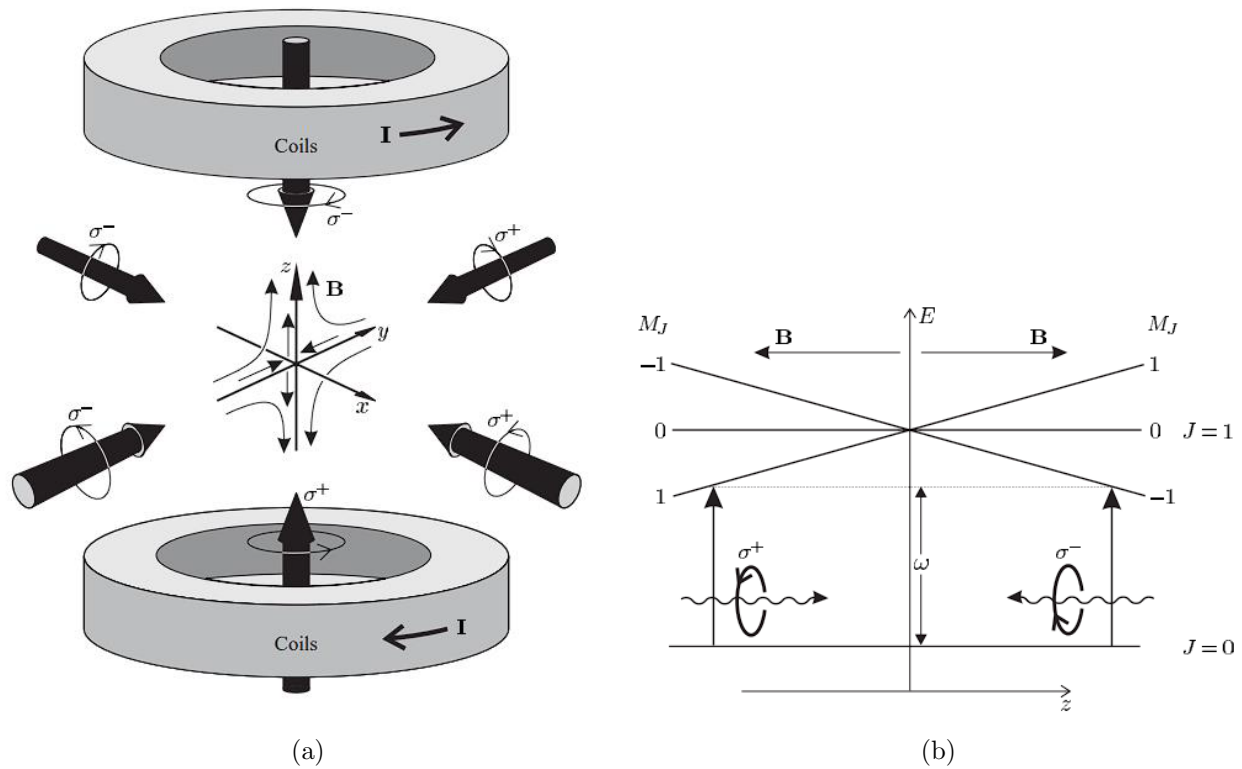


Figure 2.3: (a) The MOT setup. The large arrows represent the trapping laser beams traveling in six directions. The beams are circularly polarized to drive either the σ^+ or σ^- transitions. The quadrupole magnetic field is shown at the center of the trap. (b) This MOT works by inducing the Zeeman effect linearly with position from the center of the trap. As z increases, the energy sublevels increase or decrease in energy. The energy of the trapping light and the direction of their circular polarization are shown at the bottom of the graph. Images taken from [7].

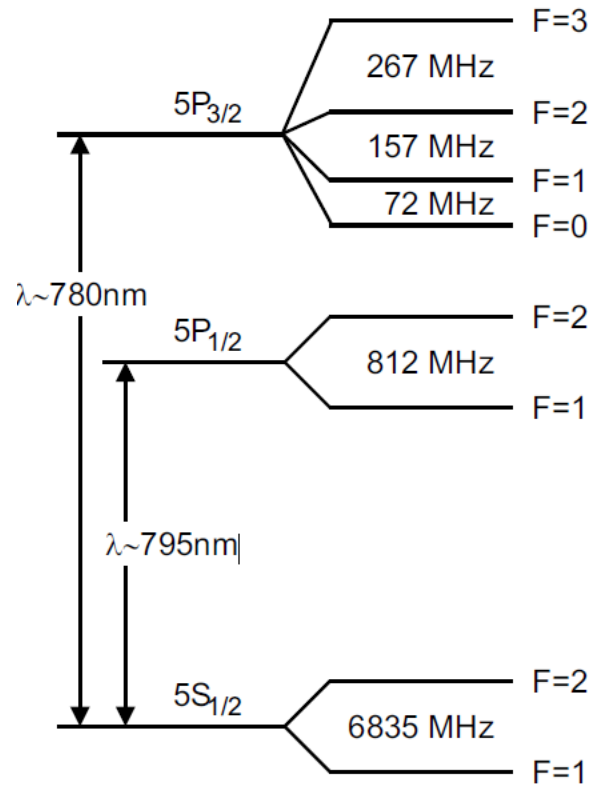


Figure 2.4: Energy level schematic of Rb-87 showing the wavelength of light between transitions. Figure taken from [6]

magnetic trap that is used to move the cloud around the vacuum system to the position of the electrostatic trap.

2.1.3 Magnetic Trap of Rb and Transportation

Once a sample of Rb is cooled and collected in the MOT, the atoms are transported into a purely magnetic trap in four steps. When the magnetic fields are turned on, the cloud will gain potential energy from the Zeeman effect that is proportional to the size of the cloud, so we begin by reducing the spatial profile of the cloud through a compressed MOT (CMOT) [6]. In the CMOT phase, the trapping laser is red-detuned and the power of the repump laser is significantly reduced to limit the scattering rate of absorbed photons and limit the repopulation of atoms in the fully stretched state [6]. This has the added effect of reducing the re-radiation pressure in the trap which could lead to trap loss, so the CMOT cloud is much denser than the MOT cloud. From there, the atoms are pumped from the $F = 2$ into the $F' = 2$ state using a circularly polarized laser beam from a 780 nm diode laser. The optical pumping laser beam only hits the atoms from one direction and is circularly polarized to drive most of the atoms to the $F = 2, M_F = 2$ state for magnetic trapping. Finally, the purely magnetic quadrupole trap is turned on by increasing the current going to the MOT coils. The magnetic fields are ramped up to a gradient of about 320 G/cm in about half of a second [6]. For a loading time of thirty seconds, we can get a consistent loading of $1.1 * 10^9$ atoms in the MOT. The MOT electromagnetic coils are mounted on a large and small track that can move in the y and z directions (Figure 2.5a). The tracks move through a servo motor with a precision of about $5\mu m$, which are connected to a computer through a shielded cable. The tracks are used to transport the trapped ultracold Rb cloud to the ultra-high vacuum section of the experiment where the molecules are trapped (Figure 2.5b).

2.2 Cold OH Generation

One of the goals of the experiment is to verify the efficiency of sympathetic cooling for the hydroxyl radical. To do this, it is important to electrostatically trap the molecules for as long as

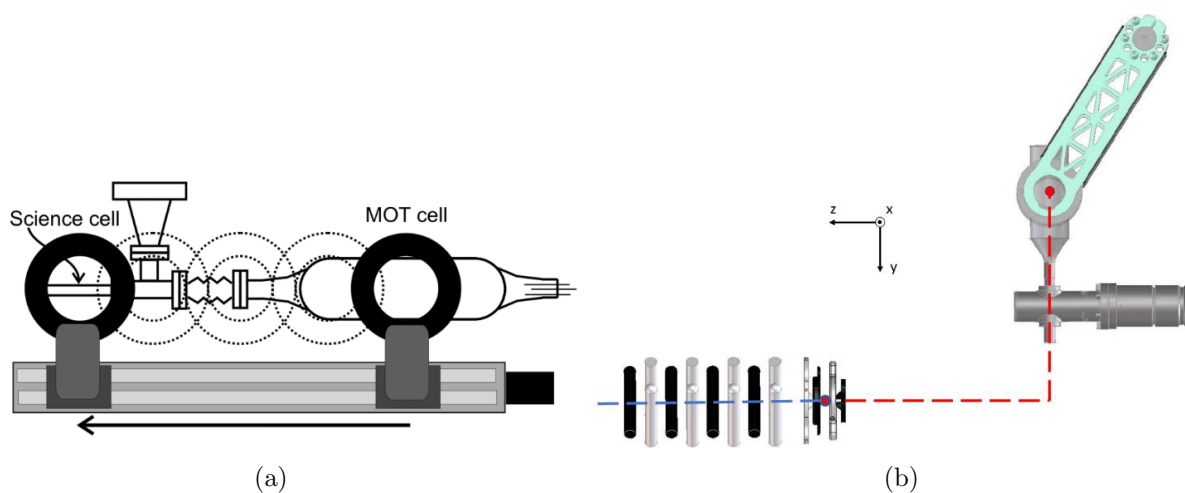


Figure 2.5: (a) Illustration of the moving magnetic trap. The MOT cell is the glass cell in which the Rb atoms are cooled and collected. The dark disks represent the magnetic coils, one on top of the cells and one on the bottom (not pictured). The track moves along the long y dimension and molecular beam direction z . Images taken from [6]. (b) Illustration of the electrostatic trap (the four electrodes on the left), magnetic trap and track (on the top right), and Stark Decelerator (series of black and white electrodes on the far left). Image taken from [3].

possible so that they can interact with the ultracold Rb for a long time. Molecules have additional degrees of freedom in vibrations and rotations, so to trap the molecules, we use supersonic expansion and a Stark Decelerator to cool the molecules. With supersonic expansion, the rovibrational states of the molecules are quenched/brought near to the ground state through collisions with krypton gas. Krypton is used since it is an inert gas and is much larger than the OH molecule. By quenching these states, we are also preventing the molecules from forming liquid droplets, meaning that the majority of the interactions for the experiment will be between the atoms and molecules, not between the molecules themselves [3]. To begin, we bubble water into the Krypton gas at high pressure until the gas mixture is 1% water, after which a voltage (about 340 V) is applied to a piezoelectric transducer (PZT) valve to release the gas into a vacuum chamber. The collisions between the water and krypton transform heat into kinetic energy, which means that when the valve is opened, the gas moves with a large velocity component in the molecular beam axis (z). The adiabatic expansion from an area of high pressure to the vacuum chamber is known as supersonic expansion, which further cools the molecules via collisions with the krypton carrier gas (Figure 2.6). At the exit aperture of the vacuum chamber, the gas is exposed to a discharge of current when we apply 1050 V to the discharge electrodes. This fragments the cooled water molecules into OH radicals, hydrogen, and electrons:



. The generated beam of cooled OH radicals then travels through a skimmer to collimate the beam. The molecular beam is then sent through a Stark Decelerator to slow the molecules enough to be trapped by the quadrupole electrostatic trap.

2.2.1 Stark Decelerator and Quadrupole Electrostatic OH Trap

We use a pulsed pin Stark Decelerator with 149 pairs of pin electrodes to create a potential that steals the molecules' forward momentum. Every fourth pin of the decelerator is electrically connected, meaning that the electric potential is periodic throughout the decelerator. Molecules that enter the decelerator in a weak electric field-seeking state experience deceleration in the follow-

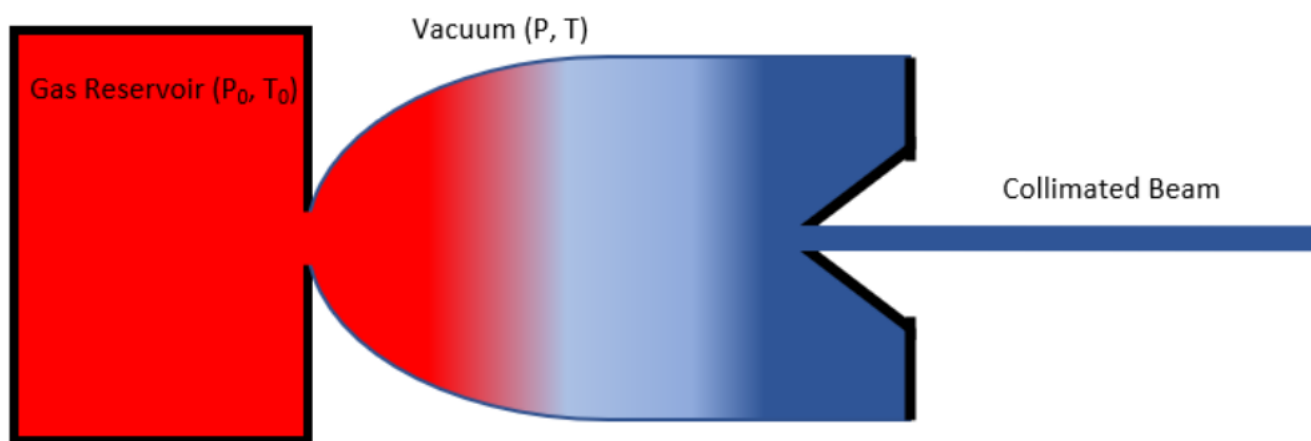


Figure 2.6: Illustration of the generation of cooled OH through supersonic expansion. Figure taken from [3].

ing way: the electrode pins create an electric field potential hill that the molecules move through and exchange their kinetic energy for Stark potential as they climb the potential hill. Before the molecules reach the peak of the potential, the electrodes are turned off so that the molecules lose that gained Stark potential. Then, the fields are turned back on in an alternate configuration so that the molecules are at the bottom of the potential hill, starting the process over again (Figure 2.7). Over repeated cycles, the molecules convert much of their kinetic energy into Stark potential energy which is removed from the system when the electric fields are switched. We use two configurations of the decelerator; a bunching signal mode where we increase the phase space density of molecules starting near a synchronous velocity or a trap detection mode where we focus on decelerating the molecules to low velocities. The former is used to optimize the system (alignment of lasers, traps, etc.) while the latter is used for collision measurements.

Once the molecules exit the Stark Decelerator, we actuate the electrostatic trap to apply a quadrupole electric field and bring the molecules to a stop at the center of the trap. Instead of just turning the trap on when we expect the molecules to be around the center of the trap, the trapping electrodes are switched on right before the molecules enter the trap, switched off, then switched back on when the molecules travel further into the trap, switched half on to further slow the molecules down, and then switched fully on when the molecules reach the center of the trap. This effectively acts as an airbag for the molecules and ensures that the majority of the molecules are at the center of the trap at rest. For collision measurements, the atoms are moved to the center of the electrostatic trap by the magnetic trap before the molecules are made and sent through the Stark Decelerator (Figure 2.5b). The Stark Decelerator and science chamber, which houses the electrostatic trap, are both under ultra-high vacuum pressures. These pressures are maintained through a series of turbo pumps.

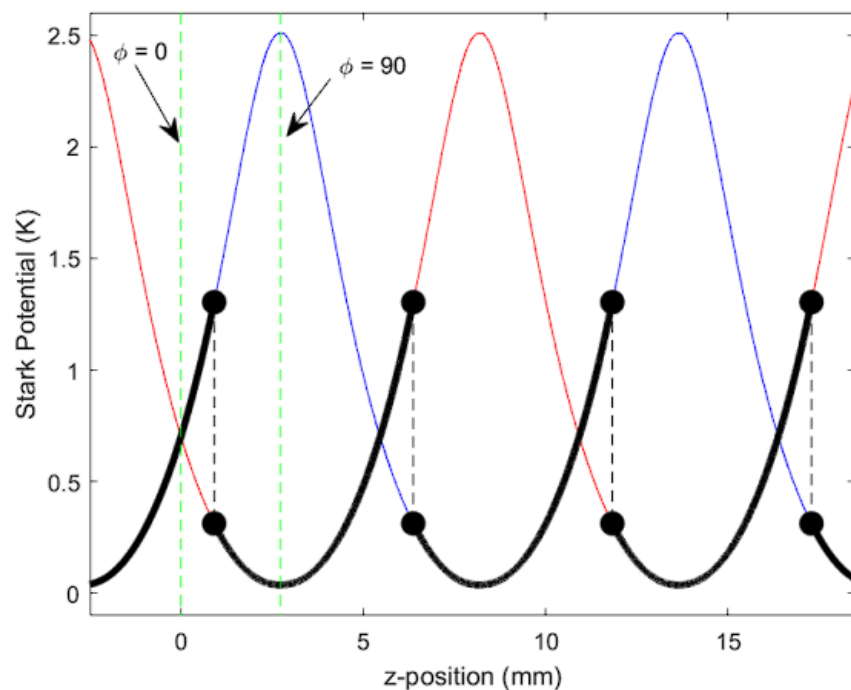


Figure 2.7: Plot of the potential generated from the Stark Decelerator electrode pins. The blue curve is the potential at the configuration where in the series of pins, the first one is set to $+12V$, the third one is set to $-12V$, and the second and fourth ones are grounded. The red curve shows the potential when the electrodes are set to an opposite configuration. The dark curve shows the molecules climbing the potentials until the electrode configuration is switched, stealing stark potential (and kinetic energy) as the molecules move through the decelerator. Image taken from [3].

Chapter 3

Characterization Methods

The detection methods that are used to understand the dynamics of the atoms and molecules in the dual trap are absorption imaging for atoms and ionization detection methods for the molecules and atoms. These methods provide the spatial distribution of the species and show how that distribution evolves. As such, detection methods are also used to align the trapped atoms and molecules to optimize interaction time.

3.1 Absorption Imaging

The spatial distribution, temperature, and total number of the trapped Rb atoms are measured through laser absorption. The entire cloud is probed with a 780 nm laser beam that is frequency-modulated by a series of acoustic optic modulators. The probe laser beam drives the $F = 2$ to $F' = 3$ transition and is coupled with imaging coils that provide the quantization axis for this transition. The cloud scatters photons out of the probe beam, creating a shadow that is focused onto a charged coupled device (CCD) array. The array is 1024 x 1024 pixels with a 16-bit resolution, each pixel measuring some intensity of light I . The column optical density (OD), or the amount of light absorbed, is given by

$$OD_{measured} = \ln\left(\frac{I_{null} - I_{dark}}{I_{shadow} - I_{dark}}\right), \quad (3.1)$$

where I_{null} is the intensity of light taken with only the probe beam present, I_{dark} is the intensity of light taken with no probe beams or atoms present, and I_{shadow} is the intensity of light taken with

both atoms and the probe beam present. However, the OD that is measured is not the true OD as any detuned light or scattered light that can't be absorbed by the atoms can also hit the CCD array. This limits the maximum observable OD. To account for this, we calculate a modified OD using the maximum observable optical density OD_{sat}

$$OD_{mod} = \ln\left(\frac{1 - e^{-OD_{sat}}}{e^{-OD_{measured}} - e^{-OD_{sat}}}\right). \quad (3.2)$$

The atoms are imaged 11.68 cm from the zero position of the large track inside the MOT cell. To avoid interference from the eddy currents generated by turning the magnetic trap off when imaging, all the absorption imaging is done in the glass MOT cell. We then apply the appropriate magnification to convert pixels to length in meters and use a 2-D Gaussian fitting routine to generate a 2-D image of the spatial distribution of the atoms. A MATLAB script is used in a LabVIEW program to do the fitting, which yields the total number of atoms, the density of the cloud, the width of the cloud in the y and z dimensions, the center of the cloud in the y and z direction, the peak OD, and the pixel intensity averages of the null, dark, and shadow images.

3.2 Ionization Technique

To characterize the OH molecules, we use the resonantly enhanced multiphoton ionization (REMPI) technique. To ionize the molecules, a 1+1' scheme is used, which means that one photon (of 281 nm wavelength for OH) is needed to excite the molecule, and one photon (of 118 nm wavelength for OH) is used to drive the molecules into an autoionizing Rydberg state [8]. We use 532 nm light from the second harmonic of a Nd:YAG laser to pump a pulsed dye laser that is frequency doubled to create the 281 nm light and the 355 nm light from the third harmonic of a separate Nd:YAG laser going through a gas mixture of argon and xenon to create the 118 nm light. Then, to detect the ions we switch the configuration of the electrostatic trap electrodes to (3, 3, 2, 0) kV to push the ions through a time-of-flight mass spectrometer (TOFMS) to a microchannel plate detector (MCP). The first ionization energy of Rb is 4.18 eV, so the 118 nm light (10.51 eV) also ionizes Rb, meaning that we can also use this technique to scan the atom cloud. The voltage signal

from the MCP detector is then sent through either a high-gain or low-gain amplifier depending on the number of ions that are expected (a high-gain amplifier for larger bunching signals of ions and a low-gain amplifier for individual ions). The transimpedance amplifiers convert the current from the MCP into a voltage that can be read. Typically, when the low gain amplifier configuration is used, the signal is sent to a multichannel scalar (MCS) to collect the number of ion signals into different time bins. This is then used in a LabVIEW routine that calculates an average number of ions over a specified bin window (time window). Since the TOFMS separates ions by time of arrival, different time windows correspond to ions of different mass.

Chapter 4

Preparation and Measurement of Collisions

4.1 Theory and Experiment Expectations

One of the most notable methods to create ultracold molecules is to use ultracold atoms to sympathetically cool the molecules. By bringing the cold molecules into contact with the much colder atoms, the second law of thermodynamics demands that heat travel from the molecules to the atoms, which will then bring the molecules to sub-Kelvin temperatures. This method has already been proven to cool trapped ions and other neutral atoms, which leaves atom-molecule interactions to be explored [9, 10]. As discussed in the introduction, the low molecule density and need for long interaction times make the dual trap a more convenient method to study sympathetic cooling over beam experiments. However, the external trapping fields of the dual trap can negatively impact atom-molecule interactions. When an elastic collision occurs, the OH molecule remains in the weak electric-field-seeking state and transfers some of its kinetic energy into the Rb atoms which act as a heat reservoir. This not only cools the molecules but also reduces the width of the molecular cloud since width is a function of temperature. On the other hand, when an inelastic collision occurs, the molecules can be knocked out of the weak electric-field-seeking state. This state is not the lowest energy state the molecules can be in, so there is a ground state for the molecules to fall into. Since the electrostatic trap only traps molecules in the weak electric-field-seeking states, an inelastic collision results in trap loss. Therefore, for sympathetic cooling to occur, the elastic collision rate must be significantly larger than the inelastic collision rate, as it only takes one inelastic collision to remove a molecule from the trap.

4.1.1 Theoretical Models for Sympathetic Cooling

Current theoretical models of the interactions between OH-Rb predict that in all temperature regimes, sympathetic cooling is unlikely for Rb and OH trapped in weak field-seeking states [5]. With OH, its permanent dipole moment points in a direction at a given moment in time, meaning that the induced polarization on the Rb atoms changes with the molecule dipole direction. As such, the potential energy surface of OH-Rb interactions is anisotropic. As a result, when a collision happens the electron spin will follow the change in the molecular axis. The anisotropy of the potential energy surface results in many collisions between Rb and OH being inelastic [5]. To calculate the inelastic and elastic cross sections of OH-Rb interactions, Lara *et al.* considered a close-coupling basis state to describe the physical states of OH-Rb interactions. The rubidium basis is given by

$$|Rb\rangle = |f_a m_{f_a}\rangle \quad (4.1)$$

where $f = s + i$ total angular momentum as the sum of i nuclear spin and s electron spin quantum numbers. The OH basis is given by

$$|OH\rangle = |s_d \bar{\lambda} \bar{\omega} \epsilon_d m_{f_d}\rangle \quad (4.2)$$

where i_d denotes the nuclear spin angular momentum of the molecule, f_d denotes the total angular momentum of the molecule as a sum of quantum numbers j and i_d with projection m_{f_d} , and the bar refers to the absolute value of the respective number. The rest of the numbers are used in linear combinations to make states of good parity [3]. Finally, the partial wave degree of freedom $|LM_L\rangle$ is considered to account for the OH-Rb orientation in the lab frame. This gives a total basis set of

$$|s_d \bar{\lambda} \bar{\omega} \epsilon_d m_{f_d}\rangle |f_a m_{f_a}\rangle |LM_L\rangle. \quad (4.3)$$

The fully stretched states that are considered for the theoretical calculation in channel 1 (C1) are

$$|OH\rangle = |\epsilon = f, f_d = 2, m_{f_d} = +2\rangle, |Rb\rangle = |f_a = 2, m_{f_a} = +2\rangle. \quad (4.4)$$

In this experiment, we trap in the

$$|OH\rangle = |\epsilon = f, f_d = 2, m_{f_d} = \pm 2, \pm 1\rangle, |Rb\rangle = |f_a = 2, m_{f_a} = +2\rangle \quad (4.5)$$

states. The cross sections are calculated in two temperature limits. The first is a higher energy limit (above $10^{-2}K$), which are best described by the semiclassical Langevin capture model [5]. The Langevin inelastic cross sections as a function of collision energy (temperature) is given by

$$\sigma_{Langevin}(E) = 3\pi\left(\frac{C_6}{4E}\right)^{1/3} \quad (4.6)$$

where E is the collision energy and C_6 is the isotropic Vanderwalls coefficient of the potential energy surface. Figure 4.1 shows Equation 4.6 plotted against the calculated inelastic and elastic cross sections, where the Langevin model seems to accurately reproduce the behavior of the cross sections in the higher energy limit. That being said, elastic and inelastic cross sections are close in magnitude in this limit, and as such we still expect the impact of inelastic collisions to make cooling inefficient at this temperature range.

In the lower energy temperature limit (below $10^{-4}K$, the elastic and isoenergetic process cross sections approach a constant number, while the cross section for exoergic processes changes as a function of $1/\sqrt{E}$ [5]. As a result, the inelastic cross section rapidly exceeds the elastic cross section as the temperature goes to zero, as can be seen in Figure 4.1. In both temperature limits, the possibility of sympathetic cooling bringing OH molecules below millikelvin seems improbable.

The cross sections calculated by Lara *et al.* suggest that in most cases, inelastic collisions will dominate the behavior of OH-Rb interactions for OH and Rb in fully stretched states. These calculations, however, don't account for some important experimental conditions. To begin with, the calculations do not account for the effects of an external electric field. An external electric field is used to trap the molecules, and as such the OH and Rb are subject to electric fields tens of kV/cm in magnitude. Electric fields are known to enhance inelastic collisions while suppressing elastic collisions [4]. In the case of ND_3 -Rb cold collisions, the electric field effect is calculated to saturate at 5kV/cm and experimentally determined to not impact the cross sections in the tested voltage range [4]. To make sure that the trapping potential in this experiment is large enough such that the electric field effect is saturated, the cross section measurement procedure can be repeated at varying electrostatic trapping potentials. The resulting cross sections can then be compared to

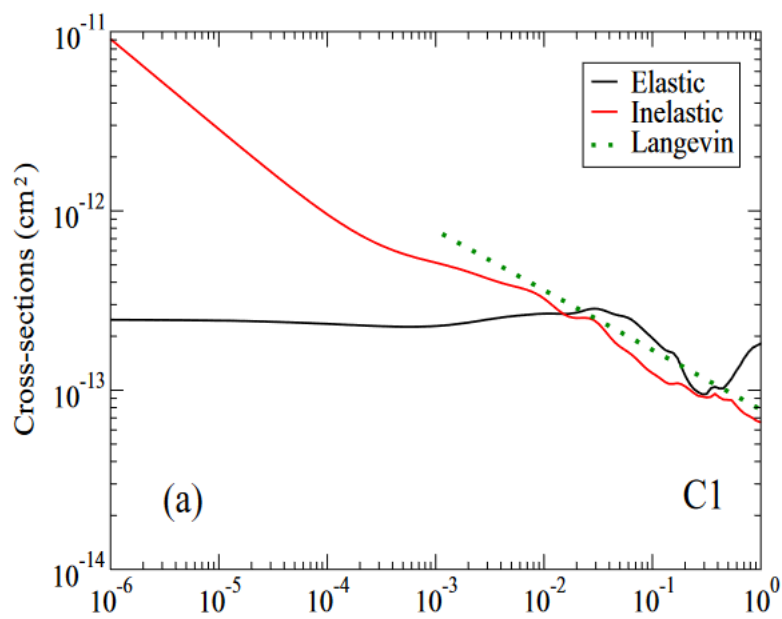


Figure 4.1: Theoretically calculated inelastic and elastic cross sections in the incident Channel 1 case. Plot also includes the Langevin inelastic cross section for the higher temperature range. Figure taken from [5].

determine the impact of the electric field from the electrostatic trap.

Furthermore, the theoretical calculations consider different OH states. For the theoretical calculations to better reflect experimental conditions, the $m_{fd} = -2, -1, +1$ states would have to be included as incident channels.

4.1.2 Cross Section Expectations

When accounting for the impact of the electric and magnetic fields from the dual trap and the interactions between ultracold Rb and cold OH, the dynamics in the dual trap become difficult to model analytically. As a result, the peak density distribution of OH as a function of interaction time is not accurately modeled by an exponential decay function. The probability of a collision is related to the product of the velocity of the OH, the density of Rb, and the inelastic/elastic cross section, where the first two change with time and temperature. However, if we consider a short time, we can model OH loss as a constant where the velocity of the OH, density of Rb, and cross sections are all held as constants in time. This will give us an order of magnitude estimation of the inelastic cross section.

The theoretical calculations from Lara *et al.* suggest that for C1, where the Rb and OH are in stretched states, the inelastic cross section is consistently greater than or comparable to the elastic cross section. This implies that sympathetic cooling is unlikely, so we expect the density distribution of OH in the dual trap to decrease over interaction time. In Gray's measurements of the OH peak density distribution over interaction times with ultracold Rb, the cloud widths of the OH were measured to remain consistent over varying interaction times [3]. Since elastic collisions are the vector for sympathetic cooling to occur, this implies that inelastic collisions are more likely to occur over elastic collisions. As such, to make an approximate model of the OH trap loss, we make the following assumptions: the ultracold Rb atoms are stationary and don't contribute to collision energy, inelastic collisions dominate so we ignore the effects of elastic collisions, the density of the Rb cloud is equal to the peak density measured through absorption images, and that the molecules move at the average velocity of the cloud. The average velocity of OH molecules decelerated using

the Stark Decelerator was measured by Gray *et al.* to be $5m/s$ [11]. Let the average velocity of the molecules be $5m/s$ and the peak Rb density be $10^{10}atoms/cm^3$. The peak Rb density was determined from absorption images of the Rb cloud after moving the cloud to the dual trap, actuating the electrostatic trap for 20 ms (to simulate collision conditions), and then taking an absorption image at the glass cell imaging location. The starting peak density distribution of the molecules is yet to be characterized, but using similar trapping and loading conditions as Gray, a similar average velocity of $5m/s$ is expected. The rate of inelastic collisions per molecule can be expressed as

$$\Gamma_{inel} = \sigma_{inel}v_{OH}\rho_{Rb} \quad (4.7)$$

where σ_{inel} is the inelastic cross section, v_{OH} is the velocity of the molecules, and ρ_{Rb} is the density of rubidium atoms. Since just one inelastic collision results in the trap losing that molecule, the lifetime of the OH due to inelastic collisions corresponds to the $1/e$ lifetime of $\tau_{inel} = \frac{1}{\Gamma_{inel}}$. Other sources that can decrease OH density are collisions with background gas and blackbody optical pumping, so let τ_{no} be the lifetime of the OH in the dual trap with no atoms. The measured lifetime of the molecules in the dual trap will therefore be equal to the sum of the lifetime of the molecules without atoms present and the lifetime due to inelastic collisions, so

$$\frac{1}{\tau_{meas}} = \frac{1}{\tau_{no}} + \frac{1}{\tau_{inel}}. \quad (4.8)$$

We then model the density distribution of the OH molecules in the dual trap by

$$n(t, x, y, z) = \frac{N(t)}{(2\pi)^{3/2}\sigma_x(t)\sigma_y(t)\sigma_z(t)} e^{-\frac{1}{2}\left(\frac{x^2}{\sigma_x^2(t)} + \frac{y^2}{\sigma_y^2(t)} + \frac{z^2}{\sigma_z^2(t)}\right)} \quad (4.9)$$

where $N(t)$ is total number of molecules as a function of time, and $\sigma_i, i \in \{x, y, z\}$ being the Gaussian widths of the molecule cloud in the lab defined x, y, z axis as described by [3]. Since we are only considering small times, we can model the number of molecules as an exponential decay function with lifetime τ_{meas} , so

$$N(t) = N_0 e^{-t/\tau_{meas}}. \quad (4.10)$$

To extract the order of magnitude estimation of the inelastic cross section, we can use Equation 4.10 instead of Equation 4.9 since we can model the change of OH number as an exponential decay with lifetimes τ_{meas} for interactions times with atoms and τ_{no} for interaction times without atoms.

We then rewrite Equation 4.7 as

$$\sigma_{inel} = \frac{\frac{1}{\tau_{meas}} - \frac{1}{\tau_{no}}}{v_{OH}\rho_{Rb}}. \quad (4.11)$$

To determine τ_{meas} , the ionization laser is set at the center of the molecule cloud to measure the distribution of the OH signal over time interacting with atoms present. The distribution is then fit to an exponential decay function where the $1/e$ lifetime is then equal to τ_{meas} . Similarly, τ_{no} is determined by fitting the distribution of OH signal over time with no atoms present.

4.2 Optimizing Alignment

Co-alignment of the atoms to the molecules and the magnetic trap to the electrostatic trap must be optimized before collision measurements can be taken. When the traps are overlapped, the atoms and molecules become subject to both magnetic and electric fields, meaning that both experience Stark and Zeeman shifts. The OH radicals have a dipole that interacts with the electric field and are not optically pumped into a state to interact with the magnetic field of the atom trap. Consequently, the Stark effect dominates the behavior of the molecules over the Zeeman shift [3]. The same can not be said for the atoms due to rubidium's polarizability, meaning that the atom can form a dipole proportional to the strength of the electric field. As a result, when the electric fields are turned on the trapped atom cloud experiences an initial fast decay of atoms until the higher energy atoms leave the dual trap. The rubidium Hamiltonian due to the Stark effect tells us that the Stark potential from the electric fields is quadratic and decreases as the magnitude of the field increases, so the Zeeman effect dominates near the center of the trap [3]. The Zeeman effect allows for the atoms to be trapped in a specific state, so when the fields are not aligned or the atoms are far from the center of the dual trap, the Stark effect dominates and results in trap loss [3]. This means that changes in the atom number as a function of atom cloud position can be

used as a diagnostic of how well the atoms, molecules, traps, and ionizing laser are aligned.

4.2.1 Ionizing Laser Alignment

To get a spatial distribution of the species from the ionization method, the final mirror in the beam path that reflects the 355 nm laser into the gas cell to generate 118 nm light is changed by a picomotor and micromotor. The picomotor pushes the mirror to change the angle at which the laser is reflected onto the gas cell and can scan the cloud vertically 6 mm in length. While picomotor scans are done, the position of the micromotor is set to its center and held constant. Suppose the center of the laser's scanning range is not aligned to the center of the trapped atoms or molecules in the vertical axis. In that case, the laser will only capture part of the cloud to ionize, which results in a lower average of detected ions. While the same principle applies to the molecular beam axis, the TOFMS accelerates ions along this axis so changing the position of the ionizing laser here also changes the time at which the ions will hit the MCP. Therefore, we select a large enough time window to detect the ions or change the time window if the discrepancies in time are too large. A micromotor is used to change the position of the ionizing laser along the molecular beam axis (holding the picomotor position constant and at its center). Because the laser propagates parallel to the lateral axis (y), there is no way to scan the cloud (and align the laser) along this axis.

The procedure we follow to align the laser to the clouds is as follows: we cool and collect a sample of Rb vapor in the MOT, transport the atom cloud into the purely magnetic trap, move the cloud using the large and small tracks to the location of the electrostatic trap, turn the electrostatic trap on to simulate collision conditions, ionize the atom cloud with the 118 nm light, collect data through the TOFMS, turn the trap and laser off and reset the track positions. We use a photodiode to capture the fluorescence of the MOT cloud as it forms and convert that signal into a voltage. After the voltage reaches a certain number, the atoms are optically pumped into the $F = 2$, $M_F = 2$ state and transported into the purely magnetic trap. Loading by voltage instead of time ensures that we can generate a consistent amount of atoms as the fluorescence of the cloud is directly

proportional to the number of atoms in the MOT.

Furthermore, the center of the molecule cloud in the vertical axis is found by scanning the picomotor with the OH in the electrostatic trap and no atoms collected or transported to the dual trap. Here, OH radicals are generated and slowed down through the Stark Decelerator in the trapping mode to get an ion signal at varying x positions. Since no atoms are loaded into the trap, the molecules can be pulsed into the trap at a much faster rate of 0.1s per shot. Ideally, the picomotor and micromotor positions that result in the best signal of ions match for both the atoms and molecules, and if they don't then the next best positions are selected.

4.2.2 Dual Trap Alignment

We optimize the alignment of the dual trap by moving the x, y, and z positions of the atom cloud within the science cell. The atom cloud x and z centers are aligned to the trapped molecule cloud x and z centers since the electrostatic trap is stationary. The first axis we align is the z-axis. If the traps are not aligned, we expect to see a decrease in the overall atom number which can best be seen through absorption imaging. Therefore, alignment begins by cooling and collecting a sample of Rb vapor in the MOT, which is then transported to the fully magnetic trap. The cloud is then transported to the science cell through the large track and towards the electrostatic trap through the small track. The electrostatic trap is then pulsed on for 120 ms. From there, the cloud is moved to the absorption imaging location back in the glass cell where an image is taken and fitted in a LabVIEW program. The final position that the small track moves the coils to (along the z-axis) is then varied, with an average of ten images taken at each small track position. The number of atoms and peak OD at each z position is taken from the fitting routine and plotted with a Gaussian fit. The position that yields the best number/peak OD (center of the Gaussian fit) is taken to be the center of the electrostatic trap and thus the optimal z position for the atoms. Ideally, this scan aligns the centers of the magnetic and electric traps along the z-axis, but the ionization laser could still be misaligned along this axis. To account for this, the z alignment is followed by a micromotor scan of the atom cloud.

Alignment of the atom cloud along the y-axis follows the same procedure as the z alignment with the only difference being that the final large track position before the clouds are moved toward the electrostatic trap with the small track is varied instead of the small track position. The electrostatic and magnetic traps roughly have cylindrical symmetry, with the magnetic trap having its strong axis along the x-axis and the electric trap along the z-axis. Since the y dimension is a weak axis for both traps, the traps should not be very sensitive to misalignment along this axis.

For the vertical alignment of the atoms, a combination of absorption imaging and ionization detection is used. Here, we begin by doing a picomotor scan of the OH to find the center of the OH cloud along the x-axis. The scan is then fitted to a Gaussian where the center of the fit is used as the center of the molecules. We then do several picomotor scans of the Rb at different atom cloud x positions. This is done to find the atom cloud x position that, when scanned with the picomotor, yields a center closest to the OH picomotor center. The x position of the cloud is controlled by sending different currents to the top or bottom electromagnetic coils. The new magnetic field gradient center then pushes the atoms toward the coil with a lower current. The reason we try to match the picomotor centers of the Rb to the OH for the x-axis alignment and not the micromotor centers for the z alignment is that the strong axis of the electrostatic trap is along the z-axis, meaning that it is enough to send the atoms to the position that gives the best number when exposed to the electric trap. Furthermore, to do a micromotor scan of the molecules, the 118 nm and 281 nm lasers used to excite and ionize the molecules must be aligned, which complicates the scanning procedure. Enough picomotor scans of Rb at different x positions are taken to create a plot of how the difference between cloud centers varies with the x position, and the x position that yields a center difference closest to zero is chosen.

Ideally, the x, y, and z degrees of freedom for the atom cloud and x and z for the 118 nm laser are orthogonal to one another. However, because the degrees of freedom are controlled by changing the large or small track or pushing mirrors, coupling of two (or more) axes is unavoidable. Consequently, even if the best parameters are selected, there is a possibility that changing the x position of the atoms could have impacted the center of the cloud along the z-axis. To account

for any variation of cloud centers, the micromotor z alignment and x alignment procedures are repeated until no variation of centers is established. At this point, we measure the lifetime of the Rb in the dual trap at the new alignment parameters as a final test of alignment. The procedure for this scan is like the z alignment procedure except that the time that the atoms spend in the dual trap location with the electrostatic trap on is varied from zero to 10 seconds. If the lifetime is near the benchmark for good interaction time with the molecules, then alignment is complete and collision data can be taken.

4.3 Collisions

Once the traps are optimally aligned, the interactions between the atoms and molecules can be studied through collision measurements. As discussed in the Cross Section Expectations section, the central column density distribution of the OH is measured (through REMPI) to calculate the collision cross sections. To capture the dynamics of collisions, we therefore interleave collision measurements with atoms present with collision measurements with no atoms present. We begin the procedure for collision measurements by trapping and cooling Rb atoms in the MOT for about 15 seconds. The atoms are then transferred to the purely magnetic trap and transported to the electrostatic trap. The change in the number of Rb atoms transported to the electrostatic trap varies shot-to-shot for less than 10%. At this stage, the electrostatic fields are actuated for 0.1 seconds. This is done to account for rubidium's DC polarizability, which induces an initial rapid decay in trapped atom number. Actuating the electrostatic trap for 0.1 seconds minimizes the impact the initial rapid decay has on OH-Rb collisions. From here, OH molecules are generated and pulsed into the Stark Decelerator, which slows and cools the OH molecular beam. Within a few milliseconds, a packet of slowed OH molecules is then brought to near-zero velocity by the electrostatic trap. The two species then interact for varying amounts of time and at the end of that time, the current going to the bottom coil of the magnetic trap is brought to zero to push the atoms down. The density of the atoms is much larger than the density of trapped molecules, so to be able to measure changes in distribution due to collisions, the column density of molecules is

used. Pushing the atoms away allows for the center column density of the molecules to be measured through the 118 nm laser. This exact procedure is then repeated to obtain a measurement of the center of the OH cloud with no atoms present by turning on a shutter for the repump beam during the MOT loading of the Rb atoms. This is done to keep the measurements with and without atoms present as consistent as possible. Each pair of shots with and without atoms takes about 50 seconds to complete. At each interaction time point, we take 60 shots with atoms present and 60 shots without atoms present.

Chapter 5

Results and Analysis

5.1 Characterization of Rb and OH

The final position of the Rb cloud (magnetic trap) and 118 nm ionizing laser were determined after multiple iterations of the alignment procedure. The lifetime of the atoms in the dual-trap was then measured as a final check of alignment before collisions were measured. Along the z-axis, the number of atoms and peak OD as a function of the small track position matched the expected behavior of a Gaussian distribution. The peak of that distribution at position 9.25 cm into the science cell was set as the optimal alignment position of the atoms along the z-axis (Figure 5.1).

When it comes to the alignment of the ionization laser to the atom cloud along the z-axis, a Gaussian distribution of the ion signal as a function of the micromotor position was not observed. The distribution is better described as a sum of two Gaussian distributions (Figure 5.2). The 118 nm ionization laser should be hitting less dense sections of the atom cloud as the micromotor shifts the beam's position along the z-axis, meaning that the average ion signal should decrease as the laser moves away from the center of the cloud. The fact that two distinct curves appear implies that the cloud is still being ionized as the 118 nm light becomes defocused, which implies that the 355 nm light used to make the 118 nm light is ionizing the cloud. However, since 118 nm light has a higher energy, more atoms are ionized by the 118 nm beam, so the spatial distribution of ions made from the 118 nm light should have a larger amplitude than the distribution of atoms ionized by 355 nm light. This means that the ionization laser can be aligned to the center of the atom cloud along the z dimension by setting the micromotor to the position that gives the center

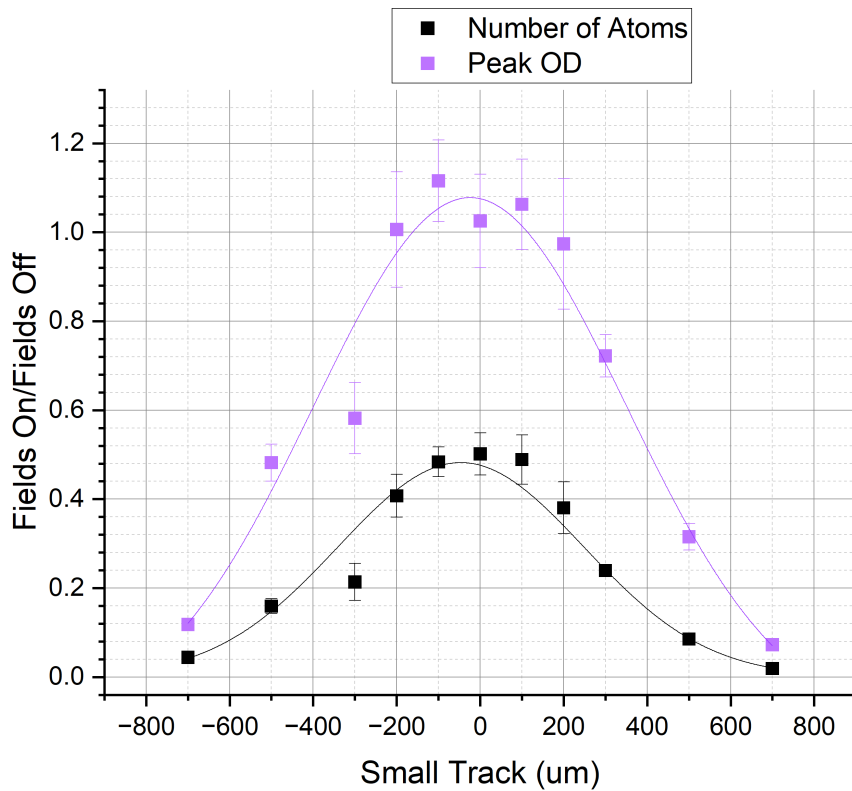


Figure 5.1: Plot of the number of atoms and peak OD at varying small track positions. The small track position is in micrometers away from the center of the electrostatic trap. Atom number and peak OD are given as a ratio of the number with the electric fields on over the number with the electric fields off at the same track position. Gaussian fits are also shown next to the data points.

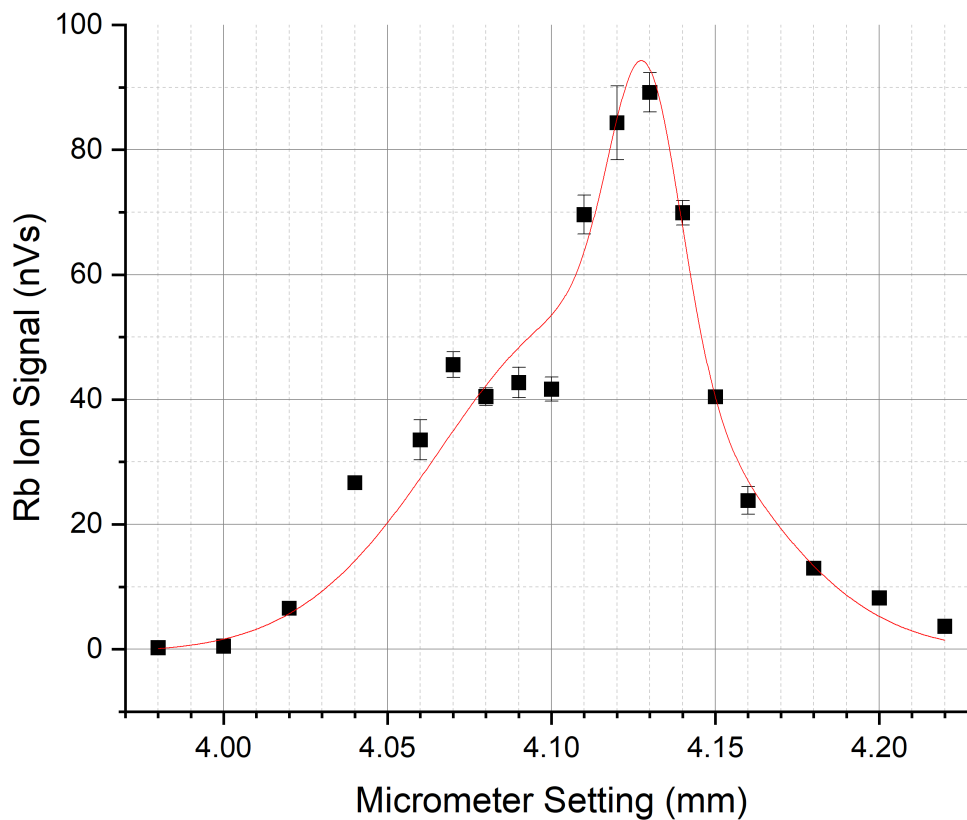


Figure 5.2: Plot of the Rb ion signal from the MCP at varying micromotor positions. The distribution of ions hitting the MCP over a short time was obtained from an oscilloscope. The area under the curve was determined to be the average ion signal (nanovolt seconds). The ion signal is fitted to a double Gaussian curve.

of the distribution due to 118 nm light curve on the double Gaussian fit. By fitting the Rb ion distribution to a double exponential, we account for any potential shifts the distribution due to 355 nm light may have on the center of the distribution due to 118 nm light.

From there, the atoms were then aligned along the y-axis. The distribution of the atom cloud taken from absorption images can be best modeled by a Gaussian distribution (Figure 5.3). Similar to the small track alignment of the atoms along the z-axis, the final position of the large track that yielded the largest number of atoms (the center of the Gaussian fit) was set as the optimal position. Using the conversion of motor steps to cm, this was determined to be 51 cm from the back of the MOT cell along the y-axis.

Then, the atom cloud and ionizing laser were aligned to the center of the electrostatic trap (and therefore the center of the molecule cloud) along the x-axis. The vertical profile of the OH taken by scanning picomotor along the x-axis resulted in a distribution that is best modeled by a Gaussian distribution (Figure 5.4a). Since the molecules are effectively stationary, the center of the Gaussian fit of the OH vertical distribution was used as the benchmark center for atom and laser alignment. From there, multiple picomotor scans of the atoms were made with the atoms at three different x positions (magnetic coil current offset 30 A, 34 A, 37 A). At a coil current difference of 34 Amps, the center of the Rb cloud and center of the OH cloud from vertical picomotor scans differed only by 0.013 ± 0.052 mm, so the atom x-position was set to 34A and the ionization picomotor position was set to -1.48 mm.

After multiple iterations of the alignment procedure were done and the atom and molecule cloud centers along the x-axis were confirmed to be on top of each other within error bounds, the lifetime of the Rb atoms in the dual trap was measured. We expect the width of the Rb cloud as a function of time spent in the dual trap to be a double exponential decay of the form

$$N_{Rb}(t) = (N_0 - N_1)e^{-t(\frac{\tau_1 + \tau_2}{\tau_1 \tau_2})} + N_1e^{-\frac{t}{\tau_2}}, \quad (5.1)$$

where N_{Rb} is the total number of atoms in the dual trap at a given time, N_0 is the initial number of atoms in the dual trap, N_1 is the number of atoms that remain trapped after the electrostatic field

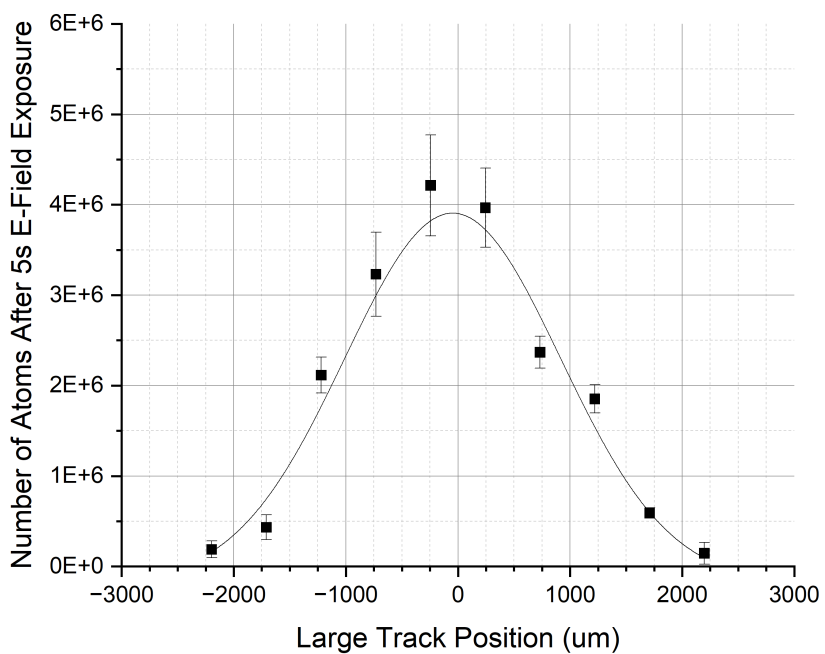


Figure 5.3: Plot of the number of atoms and peak OD at varying large track positions. The large track position is in micrometers away from the center of the electrostatic track along the y dimension.

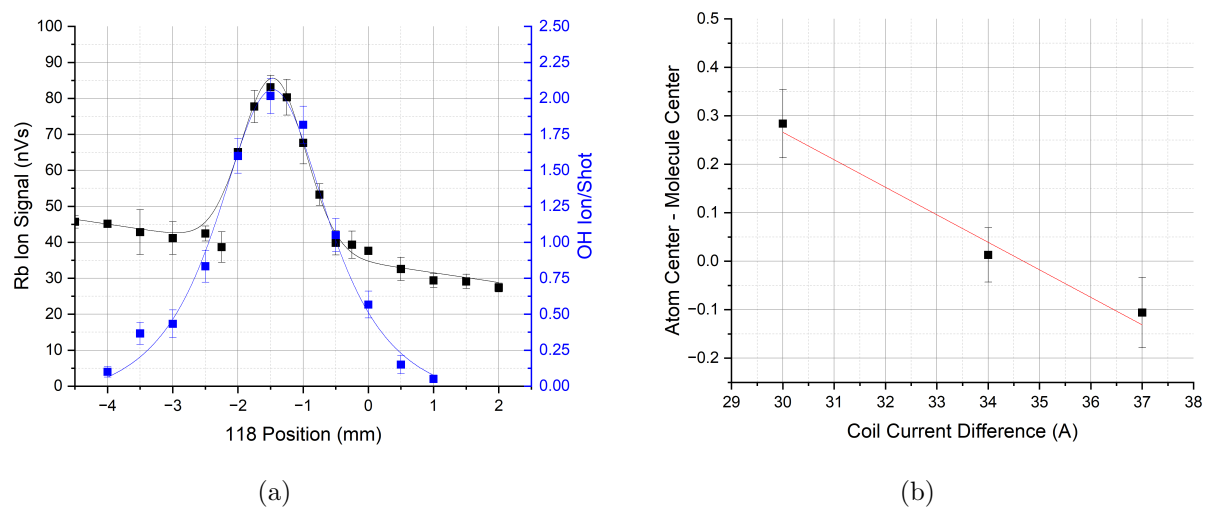


Figure 5.4: (a) Plot of the Rb ion signal (black) and OH ion signal (blue) at the atom x position that gave the best overlap of cloud centers. The atom x position was set to a coil difference of 34 A. (b) Plot of the difference of picomotor scan centers between the Rb and OH over varying x positions of the Rb cloud (controlled by the magnetic trap coil current offset). A linear fit was applied to the data to find the current offset (atom x position) that would yield a picomotor scan center difference of zero.

is turned on, τ_1 is the fast decay time, and τ_2 is the slow decay time. We use τ_2 as the lifetime of the Rb in the dual trap. The initial fast decay is due to the loss of high energy atoms from holes in the magnetic trap caused by the overlap with the electrostatic trap. In contrast, the slower decay is due to trap loss from Rb interactions with background gas. Taking the double exponential decay fit of the measured Rb atom number over trap time gave a Rb lifetime of 0.627 ± 0.093 s (Figure 5.5).

5.2 Inelastic Cross Section

With a preliminary measurement of the lifetime of Rb, we then estimated the inelastic collision cross section. This served two purposes: it was a final check that alignment is optimal and collisions are occurring and it allowed for an order of magnitude estimate of the inelastic cross section. We obtained preliminary collision measurements by measuring the center column distribution of the OH cloud with the ionization laser at two interaction times with Rb (Figure 5.6). The LabView program that is used to communicate with the OH section of the experiment uses a detect time as an analog for interaction time between the molecules and atoms. This means that for collision measurements, we can not take the detect time to be zero since the time that it takes to generate and cool the OH molecules is a part of the detect time. Instead, the initial interaction time was taken at 20 ms detect time. The other interaction time of 520 ms was determined by considering what time would be long enough to see the influence of the atoms but not so long that no OH signal would be measured. The OH signal at these two interaction times with and without atoms present were used to solve Equation 4.10 for τ_{meas} and τ_{no} . The lifetimes of the molecules with and without atoms present were determined to be 0.57 ± 0.24 s and 1.80 ± 0.15 s respectively. The lifetime of the molecules without atoms present was determined to be 3.25 standard error of means lower than the lifetime measured by Gray, while the lifetime with atoms was determined to be 1.48 standard error of means lower than the lifetime measured by Gray [3]. The calculated lifetimes along with an average OH velocity of 5 m/s and peak Rb density of $10^{10} atoms/cm^3$ were then used to solve Equation 4.11. This gave an approximate inelastic cross section on the order of

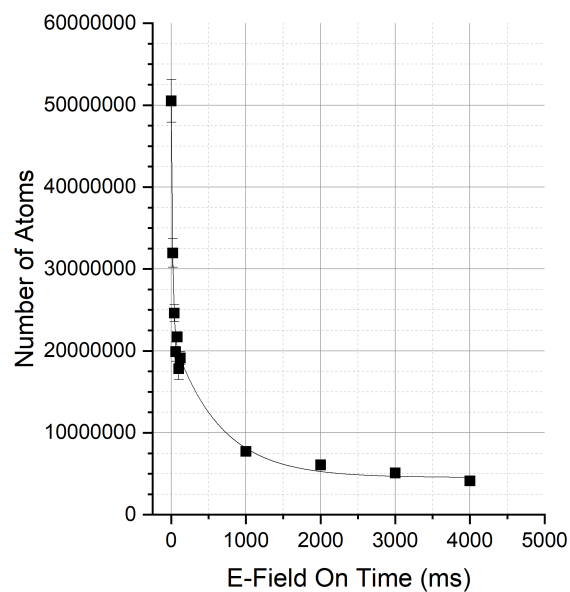


Figure 5.5: Plot of the number of atoms over varying time spent in the dual trap with both traps on. The distribution of the number of atoms is fitted to a double exponential decay curve, where the decay time of the slower decay of one curve is used as the lifetime of Rb in the trap.

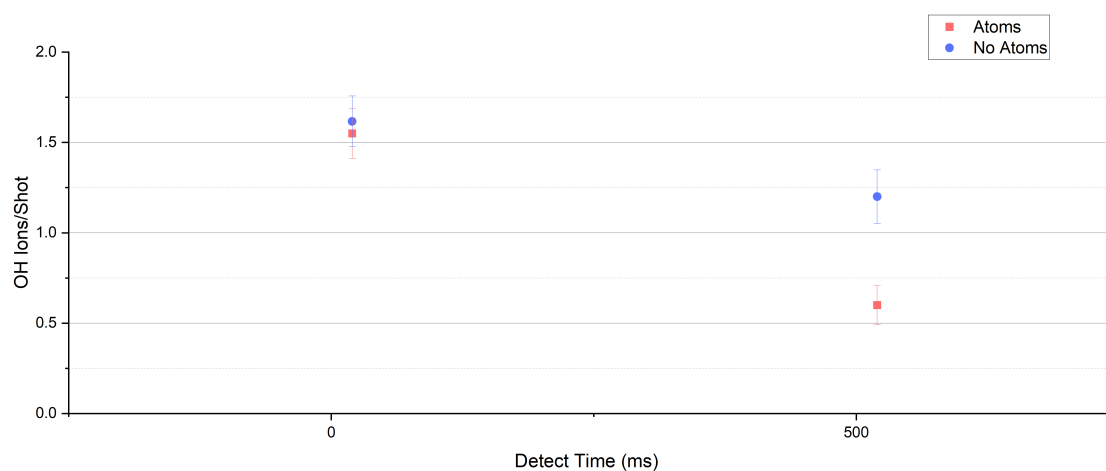


Figure 5.6: Plot of the OH signal over two interaction times with and without atoms present. Detect time is the time between the beginning of the OH creation/cooling process and the end of the experiment when the electrostatic trapping fields are turned off.

10^{-13}cm^2 , which is within the range of possible inelastic cross sections as determined by Gray [3]. Furthermore, this order of magnitude estimate is in the same order as the theoretical inelastic cross section calculated with the Langevin model by Lara *et al.*, which for a collision energy of about 50 mK was about $2 * 10^{-13} \text{cm}^2$.

The discrepancies in both of the calculated lifetimes of the molecules compared to the values calculated by Gray can be explained by the small number of interaction times observed. With a full range of interaction time measurements, the estimated inelastic cross section can be further refined in accuracy.

Chapter 6

Conclusion

6.1 Summary

In this thesis, the advantages and limitations of studying cold molecules through dual trap systems were discussed. Furthermore, the potential for sympathetic cooling between Rb and OH was explored through preliminary measurements of the inelastic collision cross sections. For the experiment, we cool and trap Rb vapor in a MOT in a vacuum chamber and then transfer the cloud into a pure magnetic trap. The magnetic trap along with the trapped atoms is then moved to overlap with the electrically trapped OH molecules. Before the overlap occurs, the molecules are created and cooled through supersonic expansion with krypton gas and slowed with a Stark Decelerator. What's more, since interaction time between the two collision partners facilitates the rate at which sympathetic cooling can happen, the alignment procedure of the atoms, molecules, and ionization laser was discussed as well. Since the laboratory axes are not truly orthogonal, the alignment procedure was repeated until no large discrepancies between trap centers were detected. We then made preliminary measurements of the Rb lifetime and collision measurements between OH and Rb. We found that the current alignment configuration results in a Rb lifetime in the dual trap of 0.627 ± 0.093 seconds. Furthermore, the order of magnitude estimation of the inelastic cross section was determined to be on the order of 10^{-13}cm^2 , which is the same order of magnitude as the theoretical cross section calculated by Lara *et al.* and within the range of calculated inelastic cross sections by Gray [5, 3]. To refine the inelastic cross section estimate, more interaction times will be taken to populate the entire range of interaction times between OH and Rb.

6.2 Future Work

As mentioned in Chapter 5.2, the preliminary measurement of collisions was done at two interaction times. This means that with more interaction time measurements, we can calculate a more statistically significant inelastic cross section estimation. However, this estimate would only bind the range of potential inelastic cross sections as the distribution of OH can not be accurately recreated by an analytical model.

Instead of an analytical model, simulations of OH-Rb interactions can be compared to measured distributions of the molecule cloud center over interaction times to extract the cross sections. Three simulations are needed to account for all of the trap dynamics of the experiment. These include preliminary simulations of the OH and Rb distribution over time spent in the dual trap with no atoms or molecules present respectively. To make sure the simulations are accurate to the experimental conditions, the distributions of atoms and molecules will be measured and compared to the simulations. The last simulation is an OH-Rb collision Monte Carlo simulation which will only have inelastic and elastic cross sections as inputs. The output of the collision simulation will then be the OH density distribution over interaction time with and without Rb present. By having the only input parameters be the two cross sections, the resulting OH distribution can be compared to the measured distribution, and the phase space of cross section combinations that replicate the observed data are then considered possible candidates for the real cross sections. A similar process was used by Fitch *et al.* to extract an upper limit for the elastic cross section between ND₃ and ⁸⁷Rb [4].

Bibliography

- [1] Jutta Toscano, H. J. Lewandowski, and Brianna R. Heazlewood. “Cold and controlled chemical reaction dynamics”. In: **Physical Chemistry Chemical Physics** 22.17 (May 6, 2020). Publisher: The Royal Society of Chemistry, pp. 9180–9194. ISSN: 1463-9084. DOI: 10.1039/DOCP00931H. URL: <https://pubs.rsc.org/en/content/articlelanding/2020/cp/d0cp00931h>.
- [2] Eric R. Hudson et al. “Cold Molecule Spectroscopy for Constraining the Evolution of the Fine Structure Constant”. In: **Physical Review Letters** 96.14 (Apr. 14, 2006), p. 143004. ISSN: 0031-9007, 1079-7114. DOI: 10.1103/PhysRevLett.96.143004. URL: <https://link.aps.org/doi/10.1103/PhysRevLett.96.143004>.
- [3] John Gray. “Measurement of Cold Molecular Collisions between Co-trapped OH and Rb”. ISBN: 9798841798774. PhD thesis. United States – Colorado: University of Colorado at Boulder, 2022. 147 pp. URL: <https://www.proquest.com/docview/2707865169/abstract/EE252FE8C3C94071PQ/1>.
- [4] N. J. Fitch, L. P. Parazzoli, and H. J. Lewandowski. “Collisions between ultracold atoms and cold molecules in a dual electrostatic-magnetic trap”. In: **Physical Review A** 101.3 (Mar. 16, 2020). Publisher: American Physical Society, p. 032703. DOI: 10.1103/PhysRevA.101.032703. URL: <https://link.aps.org/doi/10.1103/PhysRevA.101.032703>.
- [5] Manuel Lara et al. “Cold collisions between OH and Rb: The field-free case”. In: **Physical Review A** 75.1 (Jan. 5, 2007), p. 012704. ISSN: 1050-2947, 1094-1622. DOI: 10.1103/PhysRevA.75.012704. URL: <https://link.aps.org/doi/10.1103/PhysRevA.75.012704>.

- [6] H. J. Lewandowski et al. “Simplified System for Creating a Bose–Einstein Condensate”. In: **Journal of Low Temperature Physics** 132.5 (Sept. 1, 2003), pp. 309–367. ISSN: 1573-7357. DOI: 10.1023/A:1024800600621. URL: <https://doi.org/10.1023/A:1024800600621>.
- [7] Christopher J. Foot. **Atomic Physics**. Oxford Master Series in Physics. Oxford, New York: Oxford University Press, Feb. 10, 2005. 346 pp. ISBN: 978-0-19-850696-6.
- [8] Joseph M. Beames, Fang Liu, and Marsha I. Lester. “1+1 resonant multiphoton ionisation of OH radicals via the A2+ state: insights from direct comparison with A-X laser-induced fluorescence detection”. In: **Molecular Physics** 112.7 (Apr. 3, 2014). Publisher: Taylor & Francis .eprint: <https://doi.org/10.1080/00268976.2013.822592>, pp. 897–903. ISSN: 0026-8976. DOI: 10.1080/00268976.2013.822592. URL: <https://doi.org/10.1080/00268976.2013.822592>.
- [9] D. J. Larson et al. “Sympathetic cooling of trapped ions: A laser-cooled two-species nonneutral ion plasma”. In: **Physical Review Letters** 57.1 (July 7, 1986). Publisher: American Physical Society, pp. 70–73. DOI: 10.1103/PhysRevLett.57.70. URL: <https://link.aps.org/doi/10.1103/PhysRevLett.57.70>.
- [10] G. Modugno et al. “Bose-Einstein Condensation of Potassium Atoms by Sympathetic Cooling”. In: **Science** 294.5545 (Oct. 18, 2001). Publisher: American Association for the Advancement of Science, pp. 1320–1322. ISSN: 0036-8075. URL: <https://www.jstor.org/stable/3085013>.
- [11] John M. Gray et al. “Measurements of trap dynamics of cold OH molecules using resonance-enhanced multiphoton ionization”. In: **Physical Review A** 96.2 (Aug. 21, 2017). Publisher: American Physical Society, p. 023416. DOI: 10.1103/PhysRevA.96.023416. URL: <https://link.aps.org/doi/10.1103/PhysRevA.96.023416>.